JOURNAL OF GUIDANCE, CONTROL, AND DYNAMICS
Vol. 32, No. 1, January–February 2009

Deployment Control of Spinning Space Webs

Mattias Gärdsback and Gunnar Tibert*
Royal Institute of Technology, 100 44 Stockholm, Sweden

DOI: 10.2514/1.37468

Space webs are lightweight cable nets deployable in space to serve as platforms for very large structures. Deployment and stabilization of large space webs by spin have gained interest because the rotational inertia forces are in the plane of rotation and the spin rate that determines the magnitude of the web tension can be chosen to meet the mission requirements. Nevertheless, a robust control method is required for a successful spin deployment. The control law used for the deployment of the Znamya-2 membrane reflector, for which a feedback-controlled torque is applied to the center hub, was applied here to a quadratic space web folded in arms coiled around the hub. To analyze the deployment, an analytical three-degree-of-freedom model and a fully three-dimensional finite element model were developed. The simulations indicate that it is favorable to deploy the web in just one step. It is also suggested that the simple analytical model can be used to determine important mission requirements such as the torque, power, and energy required for different deployment times.

Nomenclature

A	=	cross-sectional area
E	=	Young's modulus
F	=	general force
H	=	length of the fully deployed arm ($S/2$)
J	=	moment of inertia around the rotation axis
$\mathcal{K}$	=	kinetic energy
k	=	constant parameter
L	=	current length
$\mathcal{L}$	=	angular momentum
l	=	radial position at the arm
M	=	torque
m	=	mass
N	=	tensile force
n	=	number of arms or nodes
P	=	power
R	=	position
r	=	radius
S	=	side length of the web
s	=	sign function
t	=	time
v	=	velocity
α	=	$\phi + \varphi$
γ	=	mass per length
ε	=	engineering strain
θ	=	rotation angle of the hub
ν	=	Poisson's ratio
ρ	=	density
σ	=	ultimate strength
ϕ	=	arm coiling angle
φ	=	angle between the arm and radial direction
ω	=	angular velocity

Subscripts

a	=	arm
c	=	corner
ca	=	cable
f	=	flywheel
h	=	hub
j	=	arbitrary part
n	=	node at the periphery of the hub
s	=	whole system
w	=	web
0	=	at deployment start
1	=	at deployment completion

Superscript

(i)	=	coordinate system i

Introduction

THERE is an increasing interest in the space industry to build very large structures for various applications: for example, solar panels, space antennas, and solar power systems. Many studies (e.g., [1]) conclude that structures made of flexible material have the potential to keep the package volume small and be deployed to the required size in orbit. Because flexible structures made of thin film or light cord are only capable of resisting tensile forces, some compression members are usually required. However, structures stiffened and deployed by centrifugal forces do not require stiff members to maintain their shape and offer significant advantages compared with rigid alternatives [2]: low mass, small packaged volume, low deployment power consumption, possible gyroscopic repointing, acceptable surface accuracy, and, presumably, low cost.

The interest in large space structures deployed and stabilized by centrifugal forces increased in the 1960s when Astro Research Corporation analyzed several spin-stabilized structures [3–10]. One concept is the Heliogyro solar sail (e.g., [7,8]), which uses the same principles as a helicopter for attitude control, with its flexible extendible rotor blades. The feasibility studies of a large-aperture paraboloidal-reflector low-frequency telescope (LOFT) [4,10] provide important information on deployment controllability aspects. The only successful deployment and control of a large spin-stabilized space structure is the Russian Znamya-2 experiment in 1993 [11]. The deployment process of the 20-m-diam split reflector was driven by an onboard electric motor and a counter-rotating flywheel. In 1999, the deployment of the 25-m-diam follow-up experiment Znamya 2.5 failed. To avoid similar future failures, Shpakovsky [12] proposed to first deploy the flexible membrane package radially away from the spacecraft by inflatable tubes until the centrifugal force is sufficiently large and to then let the rotational inertia forces act alone. Kishimoto et al. [13] used a similar approach. Most solar sail concepts use spin deployment and stabilization (e.g., the Interstellar Probe Mission [14,15] and the UltraSail [16]), in

Received 10 March 2008; revision received 10 July 2008; accepted for publication 15 July 2008.

*Research Associate, Department of Mechanics, Osquars Backe 18; tibert@kth.se (Corresponding Author).

which gas thrusters are planned to spin up spacecrafts to deploy and stabilize sails with 410 m and 1 km diameters, respectively. Recently, Japanese researchers have also analyzed and tested, both on ground and in space, several spin solar sail concepts [17–23].

A space web is composed of a large membrane or net held in tension by thruster-controlled corner satellites or by spinning the whole assembly. The space web concept was developed by Nakasuka et al. [24–26] for the Furoshiki satellite. An idea put forward by Kaya et al. [27] is to build up a structure by robots that crawl on the web like spiders. The difficulty in deploying a space web in a controlled manner became evident in the partly chaotic deployment during the Furoshiki experiment in January 2006 [28]. Three corner satellites were released radially by separation springs from a central satellite. Thruster control was applied on the corner satellites to reduce the repulsion force at full deployment and for attitude control. However, the web entangled due to out-of-plane motions, communication problems between the central satellite and the corner satellites, and a too rapid deployment [28]. Thus, a deployment that is easier to control is desirable. Recent studies investigate the possibilities to use centrifugal forces to deploy and stabilize the web in space [29–33].

Inspiration to mathematical models for space web deployment can be found in models for deployment of large membranes. Simple analytical models exist in which the only degrees of freedom are the center hub angular velocity, the length of the deployed web or arms, and the deviation angle of the web or arms relative to the radial axis [10,11]. Multiparticle models with spring-mass networks are also considered, with constants determined experimentally [20] and analytically [34]. However, our experience is that many experiments are required to determine a large set of constants for an arbitrary model experimentally, certainly more than for the specific case in [20]. To our knowledge, no deployment model that takes into account effects caused by the system being in orbit has been published. Most membrane deployment models (e.g., [2,11,20]) focus on the deployment of split membranes with sections that are folded on separate reels and assembled after the deployment. For space webs, it is desirable to have a continuous web to facilitate for the spider robots to crawl uninhibited. The present authors have previously presented a space web deployment concept including a prestressable web geometry and topology, a suitable folding pattern, a two-step deployment scheme, and a robust control [29,32]. In the same studies, an analytical model of the deployment of the first step of continuous quadratic space webs, folded into arms coiled around the center hub, and a finite element (FE) model, implemented in the commercial software LS-DYNA, were developed. Numerical studies on the spin stabilization of already deployed space webs have been performed by McKenzie et al. [30], Palmerini et al. [31] and McKenzie and Cartmell [33].

The aim of this study is to investigate centrifugal deployment of the space webs starting from the basic principles and, by using previous in-space experiences [11,28], to find a deployment scheme that can be used to deploy large space webs in a controlled and uncomplicated way. A new one-step deployment of the space webs, folded into radial arms coiled around the center hub, is proposed. The feedback control algorithm proposed by Melnikov and Koshelev [11] is applied to this deployment. Numerical results are obtained for the deployment of the arms with the analytical model developed in [29]. However, the analytical model cannot be used for the deployment of a complete web. Therefore, a FE model with a user-defined control torque is used for the deployment of a web in one or two steps. An approach to compute the magnitudes of the torque and power required for various deployment times is presented. Ways of applying the control torque are also discussed.

Centrifugal Force Deployment

Pros and Cons of Centrifugal Force Deployment

Use of the centrifugal forces to deploy large structures in space is appealing for many reasons:

1) Lateral stiffness is provided by the geometric stiffness induced by the centrifugal forces, and so lightweight flexible material can be used [10].

2) The rotational inertia forces dominate and are always in the plane of rotation of the spinning satellite, which keeps the out-of-plane motions of the web small [11].

3) Relatively simple control can be used to obtain a stable deployment [11]. Increased control requirements lead to more expensive equipment and increases the mission risks.

4) Deployment can be either slow or fast, whichever is suitable for the mission and leads to a controlled deployment.

5) Spinning satellites are already used for many purposes and small-scale testing can be performed on existing satellites.

There are also some disadvantages:

1) Simultaneous rotation and deployment of a large web from a tight stowed configuration always endanger web entanglement. To decrease the risk, an adequate choice of folding pattern and deployment method is required [29].

2) Oscillations occur because of the rotation. Without control, the web will coil on and off the hub like a yo-yo [34]. With control, our simulations show that in-plane oscillations occur around the equilibrium if the control is turned off before steady state is reached. Part of the excess energy may also give rise to out-of-plane oscillations [21].

3) A significant amount of energy is required if a high end velocity is desired for control or stiffness purposes.

4) The deployment time may become unacceptably long to keep the web tension and energy consumption at acceptable levels.

Conservation of Angular Momentum and Energy

A minimum of control is desirable, and free deployment is the ideal. During free deployment, the web is deployed from the initial rotation of the satellite without active control or torque added to the system. However, the expansion of a rotating system is governed and limited by two fundamental physical laws: conservation of angular momentum and conservation of energy. If the whole system rotates with the same angular velocity, the angular momentum of the system is

$$\mathcal{L}_s = J_s \omega_s \tag{1}$$

and the kinetic energy is

$$\mathcal{K}_s = \frac{J_s \omega_s^2}{2} \tag{2}$$

For the system in Fig. 1, the initial and final moments of inertia are

$$J_{s0} = J_s(t_0) = \tfrac{1}{2} m_h r_h^2 + m_w r_h^2 + 4 m_c r_h^2 \tag{3}$$

$$J_{s1} = J_s(t_1) = \tfrac{1}{2} m_h r_h^2 + \tfrac{1}{6} m_w S^2 + 2 m_c S^2 \tag{4}$$

If no torque is applied, $\mathcal{L}_s$ must be preserved. Because $S \gg r_h$, it follows from Eqs. (3) and (4) that $J_{s1} \gg J_{s0}$, and because the ratio $\omega_{s1}/\omega_{s0} = J_{s0}/J_{s1}$ is given by Eq. (1), it follows that $\omega_{s1} \ll \omega_{s0}$ and

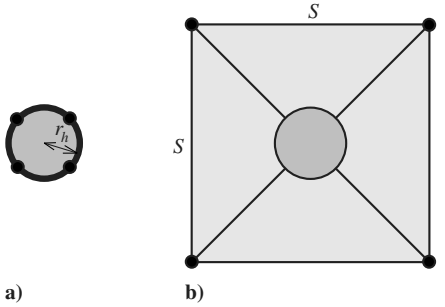

Fig. 1 The system a) before deployment and b) after deployment.

from Eq. (2) that the kinetic energy due to the in-plane rotation has decreased with the same ratio.

A simple example is useful to emphasize the preceding general conclusion. Assume that $S = 100$ m, $r_h = 1$ m, $m_c = 1$ kg, and $m_h = 100$ kg. With a 30 mm mesh width, the total weight of the Zylon web (including edge tethers) is 122 kg [29]. Inserting these values into Eqs. (1), (3), and (4) yields $\omega_{s1}/\omega_{s0} = 7.89 \times 10^{-4}$. Hence, with $\omega_{s0} = 12.6$ rad/s (2 rps), the final angular velocity is 9.9×10^{-3} rad/s or 5.7 revolutions per hour, which is too slow to be useful in practise. This value can be compared with that of the 1500-m-diam LOFT that was designed to spin with one revolution in about 11 min [4].

Thus, if the web is large compared with the hub, the angular momentum must increase during the deployment to obtain a sufficiently high final angular velocity. Furthermore, if no torque is added to the system, and because the energy must be preserved, the low final angular velocity also implies that almost all the initial kinetic energy [Eq. (2)] must be removed to avoid detrimental oscillations. The same argument can be used to show that a flywheel with an initially high rotational velocity cannot be used to apply torque to the hub and the web [11].

Control System

Fundamental Requirements

The control law should be selected so that the space web ends up in the desired configuration at the end of the deployment, within a required time period and with no undesirable oscillations or entanglements in the system. A prerequisite for a stable deployment is that the centrifugal force is much greater than the Coriolis and inertial forces [11]:

$$\frac{\omega_s L_s}{2\dot{L}_s} \gg 1 \tag{5}$$

$$\frac{\omega_s^2}{\dot{\omega}_s} \gg 1 \tag{6}$$

The condition in Eq. (5) is the most difficult to fulfill, because L_s is small and $\dot{L}_s$ is relatively large in the beginning of the deployment.

Review of Control Systems

Several control strategies for the deployment of membranes are described in the literature. However, in most cases, the focus of the study is not on the analysis of the deployment. The idea for the deployment of the Heliogyro solar sail [7] is to provide a small initial angular momentum by thrusters and then pitch the rotor blades to use the solar radiation pressure to spin up the system and deploy the blades. The deployment of the Solar Blade Nanosat [35] follows a similar scheme, in which the satellite first is spun up to 30 rpm before releasing the blades. For the LOFT system [4], a final angular velocity of 0.00916 rad/s is chosen to provide a sufficient geometric stiffness in the end, while keeping the required control torques at acceptable levels during the deployment. The LOFT system is spun up by thrusters and they continue to apply torque until approximately 60% of the 1500-m-diam reflector is deployed [4].

Hedgepeth [10] considered to use either the torque, the deployed length of radial tethers, or the tensile force in the tethers as the control parameters and concluded that a simple drag-brake type of control for the tethers is feasible with a simple two-step scheduling of the spin-up torque. This two-step scheduling consists of keeping the torque constant at approximately 200 Nm until about 40% of the deployment is complete and then rapidly decrease the torque to zero.

Mori et al. [20] performed a zero-gravity experiment of the centrifugal deployment of a clover-type solar sail. Before sail deployment the whole assembly is spun up to 4.89 rad/s by thrusters. No torque control is used, but the coiling-off-and-on phenomenon is avoided by a stick-slip clutch mechanism, which ensures that angular momentum is transferred from the central satellite to the sail, but not the other way. We consider the use of this clutch as interesting, but for larger membranes or smaller center hubs, in which more angular momentum is transferred from the hub, the hub velocity may decrease below zero, and so we conclude that an additional torque must be applied.

For the 410-m-diam solar sail in the Interstellar Probe Mission [14,15], six pie-shaped triangular segments are deployed separately. Sail deployment starts by extending three 10-m-long booms from the spacecraft. The spacecraft is spun up by gas thrusters attached to the ends of the booms. The tethers, with sail segments coiled around them, are then released and deployed by the centrifugal forces. In simulations of tether deployment [15], similar to the deployment of coiled arms, the angular velocity of the center hub is first linearly increased from zero to a maximum value and then kept constant at this value. To decrease oscillations, a structural mass damping of 5% is assumed. No details on the angular velocity of the spacecraft before the release of the sail gores or the total deployment time are given in [15]. The requirements for thruster control are not discussed.

Melnikov and Koshelev [11] decided to use the torque applied to the center hub and the velocity of the spools on which the split reflector parts are fed out from as control parameters to deploy the Znamya-2 reflector. They investigated two control laws: 1) constant angular velocity at which the coiling-off-and-on phenomenon would occur and 2) a torque with drooping characteristics, which ensures a stable deployment. The successful control law increases the torque applied to the hub as the angular velocity decreases:

$$M_h = M_{\max}\left(1 - \frac{\omega_h}{\omega_{\max}}\right) \tag{7}$$

where $\omega_{\max}$ is equal to the initial angular velocity of the system and $M_{\max}$ is only reached if ω_h decreases to zero. Melnikov and Koshelev [11] found that a higher value of the quotient $M_{\max}/\omega_{\max}$ yields a more stable deployment. Using this strategy, a high initial angular velocity, a low final angular velocity, a short deployment time, and a stable and smooth deployment without entanglement and recoiling are obtained.

A space web cannot be fed out from spools like tethers or radially split reflectors as in [11]. As a consequence, the deployment velocity cannot be controlled by the spool velocity. However, by coiling the web around the center hub, the deployment velocity is determined and controlled by the hub velocity.

Applying the Torque

Melnikov and Koshelev [11] considered two options to apply the torque for controlling the deployment of the Znamya-2 experiment:

1) Thrusters are applied both to the central spacecraft, as for the Interstellar Probe sail [14,15], and to the periphery. To maintain the thruster motion in the plane of rotation, the latter alternative would require an attitude control system for each of the peripheral thrusters.

2) A counter-rotating system driven by an electric motor is attached to the center hub. The electric motor cannot be used alone, but this system ensures that the total angular momentum is conserved and the kinetic energy can be stored in the counter-rotating system instead of creating undesirable dynamics effects such as traveling waves and oscillations in the web [11]. Once deployed, the spinning space web can also be reoriented by changing the orientation of the axis of the counter-rotating flywheel [11].

The thruster alternative was rejected by Melnikov and Koshelev [11] because it becomes more complicated, as testing and verification on the ground is difficult compared with a counter-rotating system. It has recently been proposed [36] to use the Lorentz forces from an asymmetrically charged web or hub to apply the torque, but present charging capabilities cannot create the required torque magnitudes.

Counter-Rotating Systems

Melnikov and Koshelev [11] chose the electric motor and a deployable flywheel, which increases the complexity of the system. Here, a rigid flywheel is assumed. For any flywheel, if it is spun up a priori, excess energy must be removed because the angular momentum is conserved, as discussed earlier. Contrary, this is not

necessary if the angular momentum is zero during the deployment, and in that case, the final angular velocity of the flywheel is

$$|\omega_{f1}| = \frac{J_{s1}}{J_{f1}}\omega_{s1} \tag{8}$$

It is interesting to compare this value with the maximum spin rate, with respect to material strength, for a solid disc with a small central hole [37]:

$$\omega_{f,\max} = \frac{1}{r_f}\sqrt{\frac{4\sigma}{(3+\nu)\rho}} \tag{9}$$

For a given flywheel material and with ω_{s1} determined by the required stiffness of the web, Eqs. (8) and (9) can be used to calculate dimensional requirements for a rigid flywheel. As a realistic example, we assumed a flywheel made of titanium 6Al4V alloy, with material properties $\rho = 4450$ kg/m^3, $\nu = 0.33$, $\sigma = 900$ MPa, and a stress safety factor equal to 1.3 [38]. The flywheel radius was chosen to be slightly smaller than the hub radius, $r_f = 0.4$ m, which yielded that the least possible thickness, with some safety margin, was 35 mm. For this flywheel, the mass was $m_f = 78.3$ kg and the moment of inertia was $J_f = 6.26$ kgm^2, which gave a maximum spin rate $\omega_{f,\max} = 10,320$ rpm. For a final web spin rate of 0.25 rpm, and with the same hub–web system as in the previous calculations, the flywheel had to rotate at 8917 rpm to compensate for the angular momentum of the hub–web system. At these rates, the kinetic energy of the space web was only 77 J, whereas 2.7 MJ was stored in the flywheel. Thus, for nondeployable solid flywheels, the material strength of the flywheel is not the limiting factor. Instead, a larger flywheel is preferable to decrease the energy consumption because the energy required to spin up the flywheel is much greater than the kinetic energy required for the deployment of the hub–web system.

Folding Pattern

Fundamental to a successful deployment is an appropriate folding pattern. The popular Miura–Ori folding scheme [39] used for various solar sails (e.g., [40]) is not suitable for spin-induced deployment. Hub-wrapping folding schemes for spin-deployed circular solar sails have been developed [41–45], but they provide full deployment only in theory. Furuya et al. [41] performed deployment experiments with two folding schemes and found that the ratio of deployed to full area only reached between 60 and 90%, depending on the spin rate; the centrifugal forces are simply not sufficiently large to smooth out the creases in the film. One plausible explanation for the low deployed area ratios could be that most folds in these schemes are oriented radially (i.e., parallel to the centrifugal force). Kishimoto et al. [13] attached radially oriented inflatable tubes to increase the deployed area ratio and demonstrated their efficiency through numerical simulations.

A folding scheme with folds oriented almost perpendicular to the centrifugal forces involves a two-step folding sequence. First, the membrane or web is folded to create radial arms (Figs. 2a–2d), which are then coiled around the center hub (Figs. 2e–2g). Similar schemes have previously been used by several researchers [4,11,19]. In this study, this two-step folding scheme is used for deployment both in separate steps, in which the arms are coiled off in the first step and the web is released in the second step, and for the whole web in a single step. This folding pattern is also advantageous from a modeling point of view because the first of the two deployment steps can be described with relatively few equations.

Analytical Model

Simple analytical models can be used to describe the deployment dynamics qualitatively. The development of our analytical model follows the same principles as Melnikov and Koshelev [11] used to describe the deployment of split and solid reflectors and tether systems from a rotating central satellite. Hedgepeth [10] also used a similar model for the LOFT system. The following assumptions were made:

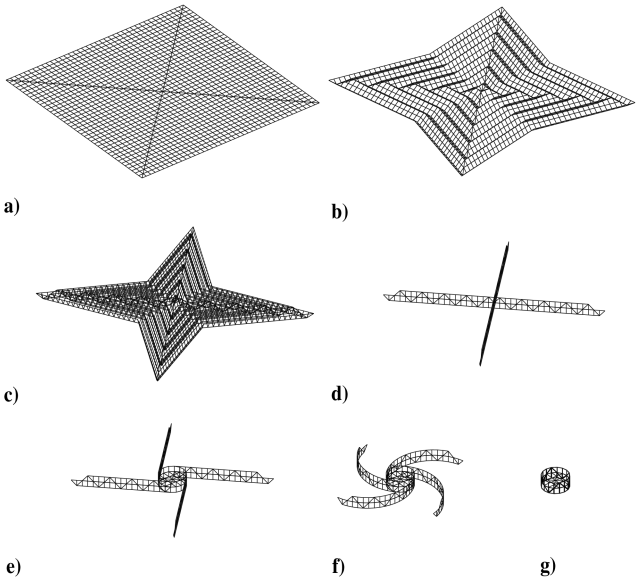

Fig. 2 Space web folding sequence.

1) Effects of the hub orbit or hub direction in the orbit were not considered.

2) Out-of-plane motions were not included.

3) The arms were supposed to be straight and deployed symmetrically relative to the central axis.

4) The gravity gradient and the elasticity in the cables were neglected.

5) Energy dissipation caused by deformation, friction, and environmental effects were neglected.

First, the coordinate systems in Fig. 3 were introduced. The change in angular momentum for the central cylinder around its axis of rotation is

$$J\dot{\omega} = M + nNr\sin\varphi \tag{10}$$

For readability, in this section, the indices for the hub and the arms are omitted: $\omega_h = \omega$, $J_h = J$, $M_h = M$, $r_h = r$, $L_a = L$, $n_a = n$, and $N_a = N$. Because stiffness and damping were not included, the equations of motion for the point mass are simply

$$\boldsymbol{F} = m_c\ddot{\boldsymbol{R}} \tag{11}$$

Its position is obtained from Fig. 3 as

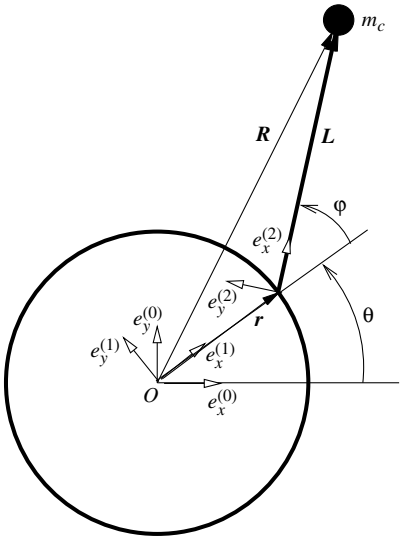

Fig. 3 Analytical model for a point mass or mass distributed in arm.

$$\boldsymbol{R} = \boldsymbol{r} + \boldsymbol{L} \tag{12}$$

and the derivatives of $\boldsymbol{R}$ become

$$\dot{\boldsymbol{R}} = \boldsymbol{\omega} \times \boldsymbol{r} + \boldsymbol{L}' + (\boldsymbol{\omega} + \dot{\varphi}\boldsymbol{e}_3^{(2)}) \times \boldsymbol{L} \tag{13}$$

$$\ddot{\boldsymbol{R}} = \dot{\boldsymbol{\omega}} \times \boldsymbol{r} + \boldsymbol{\omega} \times (\boldsymbol{\omega} \times \boldsymbol{r}) + \boldsymbol{L}'' + 2(\boldsymbol{\omega} + \dot{\varphi}\boldsymbol{e}_3^{(2)})\boldsymbol{L}' + (\dot{\boldsymbol{\omega}} + \ddot{\varphi}\boldsymbol{e}_3^{(2)}) \times \boldsymbol{L} + (\boldsymbol{\omega} + \dot{\varphi}\boldsymbol{e}_3^{(2)}) \times ((\boldsymbol{\omega} + \dot{\varphi}\boldsymbol{e}_3^{(2)}) \times \boldsymbol{L}) \tag{14}$$

where prime denotes derivation in the local coordinate system denoted by superscript (2). Projected and evaluated in the same coordinate system, the equations of motion become

$$m_c[r(\omega^2 \cos\varphi - \dot{\omega}\sin\varphi) - \ddot{L} + L(\omega + \dot{\varphi})^2] = N \tag{15}$$

$$r(\dot{\omega}\cos\varphi + \omega^2 \sin\varphi) + 2\dot{L}(\omega + \dot{\varphi}) + L(\dot{\omega} + \ddot{\varphi}) = 0 \tag{16}$$

Space webs folded into radial arms, for which the mass is distributed along the arm, can be described similarly. Deployment was assumed to be performed in two steps. The first step, the deployment of the arms, can be modeled, whereas the second step, the deployment of the web surface, is impossible to model accurately with this type of model. The space web is first folded into n identical arms positioned symmetrically around the center hub. The arms can be folded on spools at the end of the arms in a zigzag pattern or coiled around the center hub [11]. The mass per length of an arm varies linearly, starting from zero at the tip of the arm. If the arm is initially coiled around the center hub, the mass per length of the deployed part of the arm is

$$\gamma = \frac{2m_w}{nH^2}(L - l) \qquad (0 \le l \le L) \tag{17}$$

Integration over the current arm length yields the equations of motion:

$$\frac{2m_w}{nH^2}\left[\frac{L^2}{2}(r(\omega^2\cos\varphi - \dot{\omega}\sin\varphi) - \ddot{L}) + \frac{L^3}{6}(\omega + \dot{\varphi})^2\right] = N \tag{18}$$

$$\frac{L^2}{2}(r(\dot{\omega}\cos\varphi + \omega^2\sin\varphi) + 2\dot{L}(\omega + \dot{\varphi})) + \frac{L^3}{6}(\dot{\omega} + \ddot{\varphi}) = 0 \tag{19}$$

For an arm-folded space web with point masses in the corners, the equations of motion are added together, so that

$$a(r(\omega^2\cos\varphi - \dot{\omega}\sin\varphi) - \ddot{L}) + bL(\omega + \dot{\varphi})^2 = N \tag{20}$$

$$a(r(\dot{\omega}\cos\varphi + \omega^2\sin\varphi) + 2\dot{L}(\omega + \dot{\varphi})) + bL(\dot{\omega} + \ddot{\varphi}) = 0 \tag{21}$$

where

$$a = a(L) = m_c + \frac{m_w L^2}{nH^2} \tag{22}$$

$$b = b(L) = m_c + \frac{m_w L^2}{3nH^2} \tag{23}$$

To simulate space webs that are coiled around the center hub (Fig. 4), first note that $\varphi = \pm\pi/2$ (and $\dot{\varphi} = \ddot{\varphi} = 0$) when the arms are coiled around the hub. Then introduce the arm coiling angle ϕ, which is initially equal to $\pm(H/r)$ for a completely coiled arm. When the arms are completely coiled off, Eqs. (20) and (21) can be used again, with $\varphi = \pm\pi/2$ at the transition. The current length of the coiled-off part of the arm is

$$L = H - r|\phi| \tag{24}$$

and the angular velocity of the coiled-off arm is

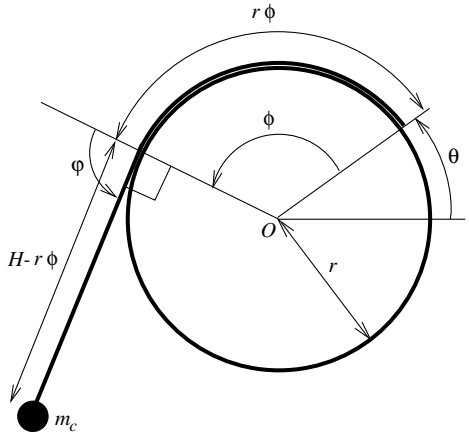

Fig. 4 Analytical model for an arm coiled around the hub.

$$\omega_a = \omega + \dot{\phi} \tag{25}$$

It follows that $\dot{\omega}_a = \dot{\omega} + \ddot{\phi}$, $\dot{L} = -\text{sign}(\varphi)r\dot{\phi}$, and $\ddot{L} = -\text{sign}(\varphi)r\ddot{\phi}$. Finally, introduce $s_\phi = \text{sign}(\phi) = \text{sign}(\varphi)$, and the equations to solve for the coiled arms become

$$J\dot{\omega} = M + s_\phi \cdot nNr \tag{26}$$

$$-s_\phi \cdot ar\dot{\omega} + b(H - r|\phi|)(\omega + \dot{\phi})^2 = N \tag{27}$$

$$s_\phi \cdot ar(\omega^2 - \dot{\phi}^2) + b(H - r|\phi|)(\dot{\omega} + \ddot{\phi}) = 0 \tag{28}$$

For a deployment that involves both coiled and coiled-off arms, it is convenient to introduce the variable

$$\alpha = \phi + \varphi \tag{29}$$

Equations for many other deployment schemes and web or membrane geometries can be derived similarly [11,29].

Finite Element Model

A three-dimensional finite element model including the center hub, the web, and four corner masses was implemented. However, the center hub was constrained to move around its center axis; thus, the center hub motion was two-dimensional. The node and element geometry and connectivity were generated in MATLAB [46]. The equations of motion were then solved in LS-DYNA [47] using the central-difference method for explicit time integration.

The main differences compared with the analytical model are that deployment sequences other than arm deployment can be studied with the FE model, the arms are not necessarily straight during the deployment, the cables can store elastic energy, and perturbations can be studied. The gravity gradient and energy dissipation can be included, but have been considered to be small for membranes in comparison with the rotational forces [11] and should be even smaller for a web. The effects of the hub orbit and hub direction in orbit are interesting, as discussed in [31], but were not a topic of the present study.

The progression of a spin deployment is highly dependent on the folded configuration. In addition to providing the initial geometry, several other problem characteristics are also due to the folding:

1) The initial velocities of all parts are proportional to their distances to the rotation axis; that is, the initial conditions depend on the folding.

2) The forces between the center hub and the web during the deployment depend strongly on the current web formation and the current tension in the web; that is., the forces applied to the web depend on the folding.

3) The boundary conditions depend, in some sense, on the folding because some parts of the web constrain others from moving.

As a consequence, the accuracy of a FE model is strongly dependent on how well the modeled folded configuration coincides with the real one. In some respects, the modeled configuration may be too perfect, and in other respects, the computational cost puts limitations on the model. Nevertheless, because it is difficult to analytically predict the deployment of a web or membrane, the FE model serves as a valuable second analysis step after the analytical arm deployment model.

In reality, the mesh width of the web would be at most 30 mm and the amplitude of swaying motions would be very small. In the finite element model, a significantly larger mesh width, 2.5 m, was used for computational efficiency. Having a single truss element between two nodes disregards the lateral inertia of the cable, and so multiple truss or beam elements are often used in dynamic analyzes. Here, only one truss element was used to connect two nodes, because dividing the cable into more truss elements would allow in-plane swaying motions that would not be present in reality. It is proposed [1] that cables are best modeled with truss elements and a material with no-compression properties to model cable slackening under compressive loads. Therefore, the cables were modeled here as truss elements with pin-jointed ends. This truss element is based on a corotational formulation, and the internal force for the no-compression material is computed as [48]

$$N_{\text{ca}} = \max(E_{\text{ca}} A_{\text{ca}} \varepsilon, 0) \tag{30}$$

Formulation (30) does not take into account the changes of volume and cross-sectional area, which were considered to be negligible in this case because of small strains.

The proposed folding scheme assumes that the cables can be bent only at the nodes and that the distance between the fold lines is twice the mesh width. These choices mean that the radius of the hub, which fits in the central deployed part of the web (Fig. 5b) is dependent on the mesh width. Thus, for a coarse web, the hub radius is unrealistically large, but still adequate for evaluating the spin deployment of the space web. This artificial constraint on the hub size is difficult to overcome, because a certain number of the web elements must be attached to the center hub to accurately transfer the angular momentum from the center hub to the web. The governing equations of the folding scheme are given in [29].

The center hub was modeled as a cylinder with rigid material. It was divided into 16 identical pentahedrons to achieve the cylindrical shape. However, this did not increase the computational cost for the dynamical analysis because the hub was constrained to move as a rigid body. In the corners, point masses were considered to be sufficiently accurate, because the contact between them and the web was not considered to be important. The contact between the cables and the rigid center hub was modeled using the kinematic constraint method [49]. This contact is completely inelastic and the contact assumption implies that cables in contact with the hub follow the hub. It is not obvious how to coil the web near the hub and include initial contact. Therefore, contacts between cable elements in the space web

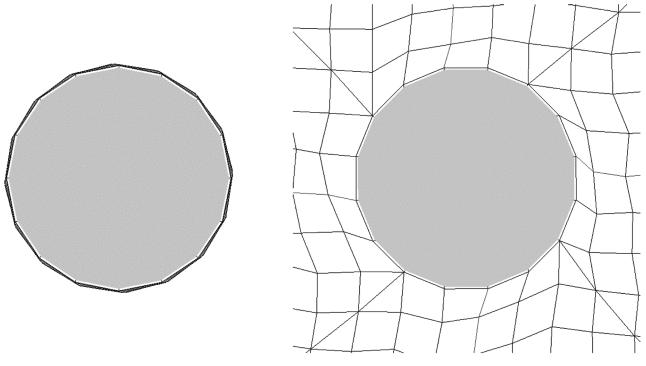

a) b)

Fig. 5 Hub–web at the initial (a) and final (b) stages.

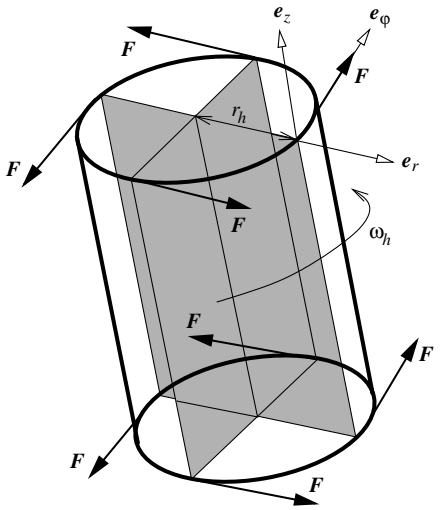

Fig. 6 Torque applied as forces on extra shells in the FE model.

were disregarded, because higher priority was given to the coiling of the space web as close to the center hub as possible (Fig. 5a).

The control torque depends on the angular velocity of the center hub, and because the angular velocity varies with time, the control cannot be specified without special treatment in FE software. In the object version of LS-DYNA, the user can implement a function in the source code that applies a force to shell or beam elements [50]. The user predetermines some parameters for this function, and at each time step, the program supplies values of, for example, the position, velocity, and accelerations of the nodes in the element. Therefore, to apply the torque, four planar shells with negligible mass were symmetrically positioned in the center hub (Fig. 6). Four shells were chosen to distribute the small mass evenly and because the velocity of the center is required. The nodes of each shell were put at the top and bottom of the center hub, 2 at the axis of rotation and 2 at the periphery at the same point as the center of the arms. From the control moment in Eq. (7), the forces on the nodes on the shells can be calculated as

$$F = \frac{M_{\max}}{n_n r_h}\left(1 - \frac{\omega_h}{\omega_{\max}}\right) \tag{31}$$

Here, eight peripherical nodes were used. $M_{\max}$, $\omega_{\max}$, r_h, and n_n were defined as user parameters. The angular velocity was calculated from the velocities and positions of the two nodes at the rotation axis and one of the peripherical nodes. First, a local cylindrical coordinate system $(\boldsymbol{e}_r, \boldsymbol{e}_\varphi, \boldsymbol{e}_z)$ was set up. Then ω_h was determined from

$$v_{n\varphi}\boldsymbol{e}_\varphi = \omega_h \boldsymbol{e}_z \times r_h \boldsymbol{e}_r \tag{32}$$

where $v_{n\varphi}$ is the velocity of the peripherical node, relative to the corresponding node on the rotation axis, projected along $\boldsymbol{e}_\varphi$.

Results of Deployment Simulations

Several different deployment simulations of a large quadratic space web were performed. In all the simulations, the web was folded as in Fig. 2. The following data were assumed: the side length $S = 100$ m, the mass of the center hub $m_h = 100$ kg, the radius of the center hub $r_h = 6.3$ m, the mass of the web $m_w = 122$ kg, and the mass in each corner $m_c = 1$ kg. The web mass was obtained by assuming that the cables were made of the Zylon fibers in [51] and that the mesh width of the web was 30 mm. For the FE model, the elastic modulus of the Zylon cables $E_{\text{ca}} = 180$ GPa, the density of the cables $\rho_{\text{ca}} = 1540$ kg/m^3, the cross-sectional area of the cables $A_{\text{ca}} = 2.5/0.030 \cdot 0.123$ mm^2, and the mesh width of 2.5 m were also included. Note that the cross-sectional area was adjusted so that the total mass of the web in the FE model was equal to that of a real web with a 30 mm mesh width.

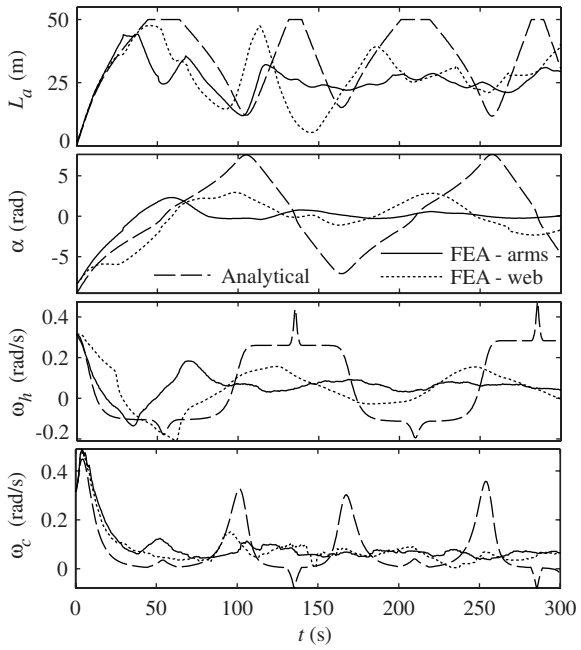

Fig. 7 Uncontrolled deployment of arms and space web.

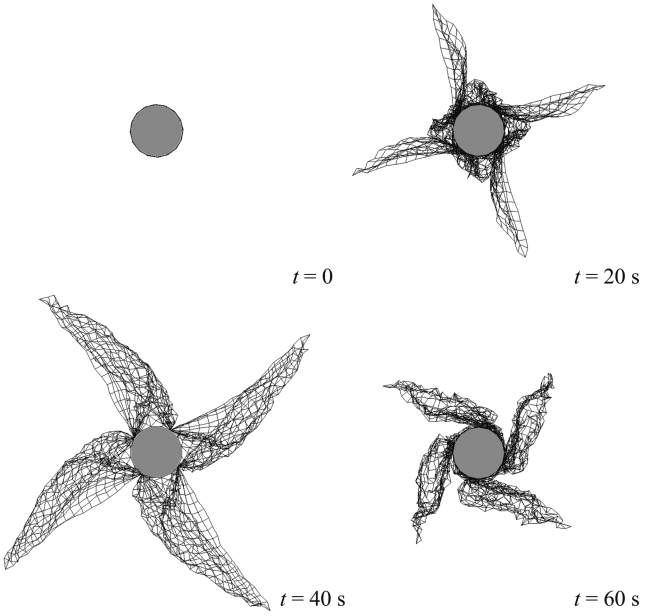

Fig. 8 Uncontrolled deployment of arms.

The results are presented with at least four graphs in each figure. The graphs show the length of the deployed arm, L_a, the coiling angle plus the angular deviation from the radial direction, $\alpha = \phi + \varphi$, the angular velocity of the center hub, ω_h, and the angular velocity of the corners, ω_c. The torque applied to the center hub is shown in a fifth graph in cases in which the control law in Eq. (7) was used.

Uncontrolled Deployment of Star Arms and Web

The first simulations involved uncontrolled deployment, for both arms and a complete web. The deployment was initiated by an initial rotational velocity of $\pi/10$ rad/s for the system, and no control was used. The initial angular velocity was chosen to obtain a realistic initial deployment velocity; that is, it was smaller than expected in reality to compensate for the greater hub radius in the FE model. During the coiling-off period, from $t = 0$ to 30 s, the analytical and finite element analysis (FEA) curves for the arm deployment almost coincide (Fig. 7). The hub direction then changed and the arms coiled back onto the center hub because of the conservation of angular momentum. As a consequence, the agreement between the two models degenerates because the arms were not straight and in tension (Fig. 8), which is one of the assumptions of the analytical model. However, it is not the aim to model the behavior after the failure, and both models describe the same fundamental behavior (i.e., that uncontrolled deployment of a large web is not possible for these data). The coiling-off-and-on phenomenon is also observed in simulations by Miyazaki and Iwai [34] for a circular spinning solar sail. For arbitrary data, Bergamin and Izzo [36] linearized Eqs. (10), (18), and (19) around $\varphi = \dot{\varphi} = 0$ and showed that the system will not converge to the equilibrium if no torque is applied.

Linearly Increased Rotational Velocity

A better test to compare the analytical and FE models was performed using a simple control strategy. It is proposed [15] to use linearly increasing ω_h from 0 at time $t = 0$ to $\omega_{\max}$ at time $t = \Delta t$ and to then keep the angular velocity constant at $\omega_{\max}$ to deploy tethers similar to the arms. No systematic way to choose these parameters is presented, but it is suggested that ω_h should linearly increase until the arms are deployed [15]. Here, the values $\omega_{\max} = \pi/10$ rad/s and $\Delta t = 75$ s were chosen. The arms were coiled off the center hub, but not completely coiled back on the hub again (Fig. 9). However, the strong oscillatory behavior of the arms, indicated by the oscillations of the parameter α, is unacceptable. This deployment scheme is also undesirable because of the high end velocity that unnecessarily increases the energy consumption.

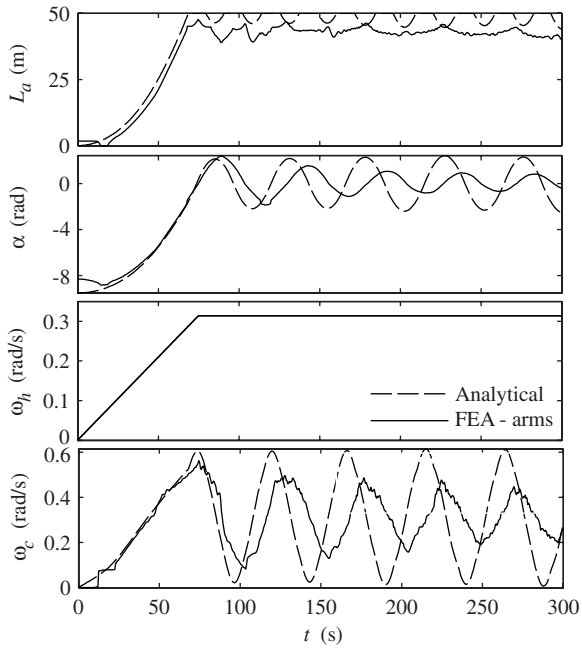

Fig. 9 Deployment of a space web with linearly increasing angular velocity.

Controlled Two-Step Deployment

For the controlled two-step deployment, a torque equal to that in Eq. (7) was applied with $M_{\max} = 126$ Nm and $\omega_{\max} = \pi/10$ rad/s. These parameters were chosen, as will be discussed later, to get a deployment time of approximately 100 s for the whole web. The analytical and the FE models show similar deployment behavior during the first step of the two-step deployment (Fig. 10). Some differences can be observed due to difficulties in folding the web and attaching it to the hub so that it is deployed in perfectly straight arms. However, both models show that a stable deployment of the arms can be achieved. Thus, no additional tethers or brakes are necessary to control the deployment velocity in the first step.

Also included in Fig. 10 are curves showing the results when the second step was initiated at $t = 90$ s, for unchanged $M_{\max}$ and $\omega_{\max}$

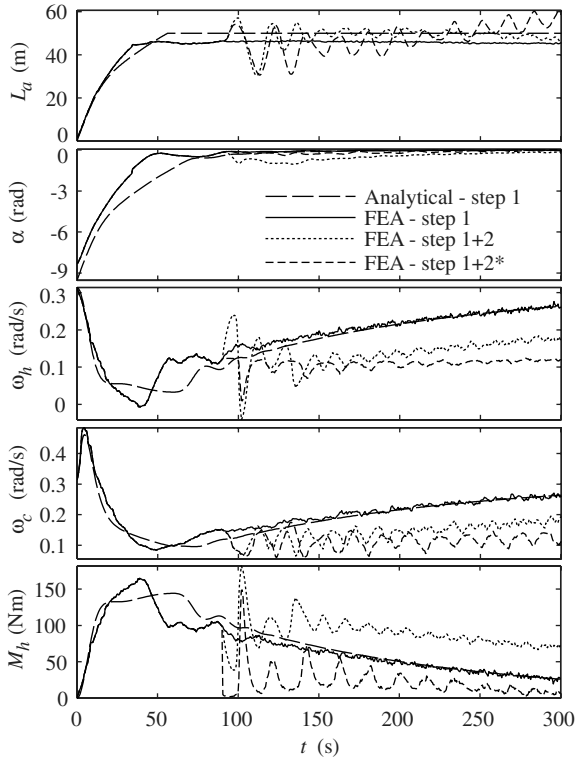

Fig. 10 Controlled two-step deployment of the space web.

(step 1 plus step 2) and for $M_{\max} = 1260$ Nm and $\omega_{\max} = 0.125$ rad/s (step $1 + 2^*$) (i.e., the angular velocity when the second step was initiated). Note also that larger $M_{\max}$ requires a high torque even for small perturbations from $\omega_{\max}$ and did not lead to a controlled deployment. The first step was considered to be completed at $t = 90$ s, because then L_a was near H, α was near 0, and ω_h was still at an acceptable level. Unfortunately, the second step was more difficult to control for both cases, partly because of its more rapid progression, but also because the web was not in tension after the initiation of this step at $t = 90$ s and forward (Fig. 11). The web was thus uncontrolled during this time because very little angular momentum was transferred from the hub to the web, even though torque was applied to the hub. However, after the large initial oscillations, the web stabilized, but ω_h had increased to an unacceptable value (Fig. 10). Additional tethers must be used for deployment length control to overcome the oscillations and prevent springback [11].

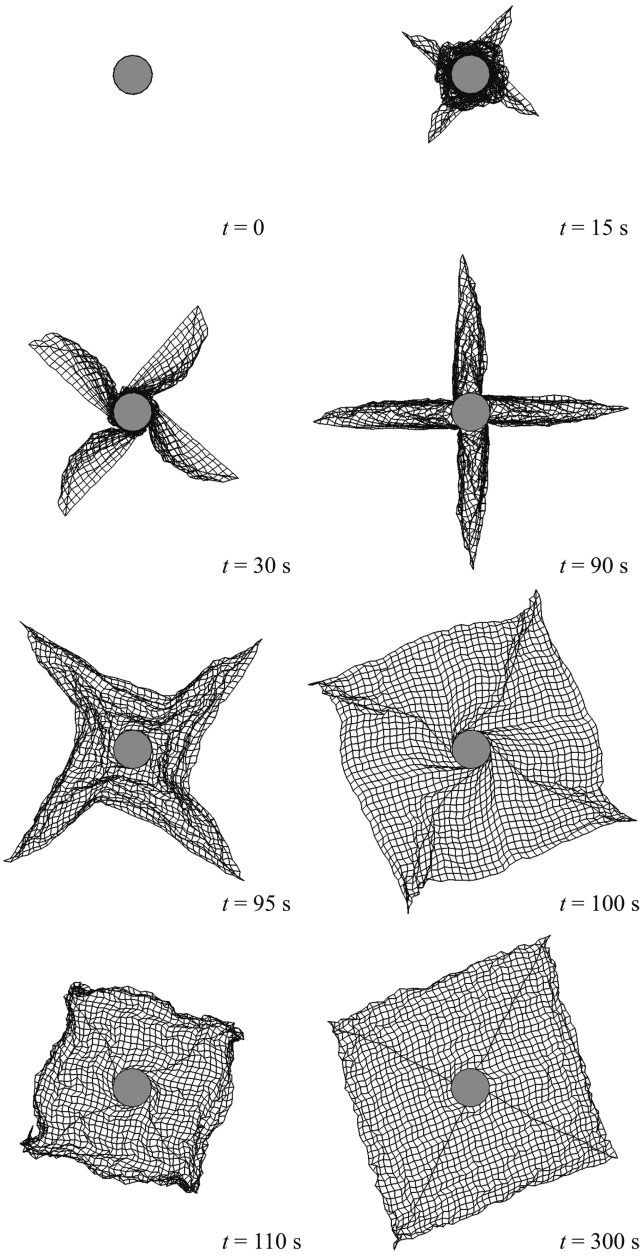

Fig. 11 Controlled two-step deployment of the space web.

Controlled One-Step Deployment

An alternative option is to deploy the web in just one step. The main advantages of the one-step deployment compared with that with two separate steps are as follows:

1) The deployment is smooth because the arms are mostly in tension and web parts that are free to move will do so.

2) No extra equipment is required to fix parts of the web for arm-only deployment or to determine when to initiate the second step.

The same control law, with $M_{\max} = 126$ Nm and $\omega_{\max} = \pi/10$ rad/s, was used for the one-step deployment of the web (Fig. 12). During the first 33 s the web was deployed as arms, then a phase followed in which the web expanded freely. At $t = 100$ s the tethers connected to the corners of the web were completely deployed (see also parameter L_a in Fig. 13), but the web was not in tension because the value of α was too high. The tension in a web increases until α is equal to zero; satisfactory tension was obtained here near $t = 200$ s.

Because a low final angular velocity is desired to minimize energy consumption, it is necessary to turn off the torque at some point, as the control law in Eq. (7) provides torque until $\omega_h = \omega_{\max}$. When the torque was turned off (e.g., at $t = 100$ and $t = 200$ in Fig. 13), the system began to oscillate, and the magnitude of the oscillations was proportional to the value of φ ($=\alpha$) at torque turn-off. The same phenomenon occurs for arms when the torque is turned off and can be explained by the analytical model. The following conditions hold when the arms are deployed and the torque is turned off: $L_a \gg r_h, L_a$ is constant, and $M_h = 0$. Equations (10), (20), and (21) can then be simplified:

$$J_h \dot{\omega}_h = n_a N_a \sin\varphi \tag{33}$$

$$N_a = bL_a(\omega_h + \dot{\varphi})^2 \tag{34}$$

$$\ddot{\varphi} = -\dot{\omega}_h \tag{35}$$

The centrifugal force is almost constant when the web is completely deployed and, consequently, N_a can be assumed to be constant. Unless $\varphi = 0$, the right-hand side of Eq. (33) is not zero, which is a requirement for steady state, and so we assume that φ is small. Then insert Eq. (35) into Eq. (33) to obtain an equation of the form $\ddot{\varphi} + k\varphi = 0$, which is the equation for a spring without damping. As a

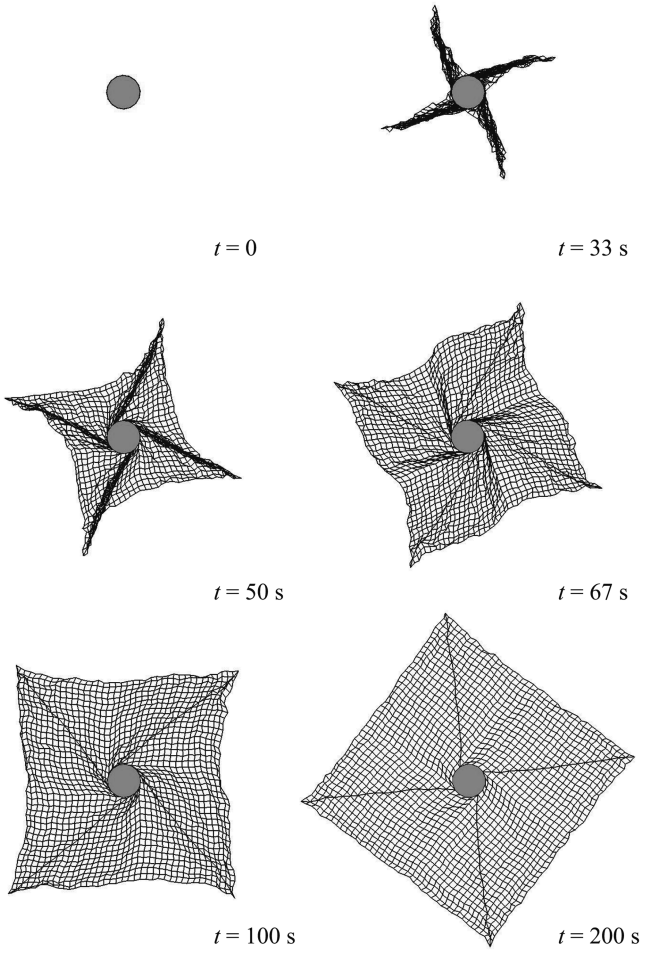

Fig. 12 Controlled one-step deployment of the space web.

consequence, the arms will continue to oscillate forever if no other effects are present. This shows that the oscillations are due to the rotational inertia forces and not due to the elasticity in the web. However, in reality and in the FE model, the small oscillations are damped out, which is shown by the decreasing amplitude of the oscillations of α and ω_h for the FE simulations in Fig. 13.

Torque and Power Requirements for Controlled Arm Deployment

The analytical model can be used to determine the torque and power required to obtain a controlled arm deployment for a given deployment time, t_1. It is interesting to use different initial angular velocities $\omega_{\max}$ and center hub radii r_h, because the initial deployment velocity is determined by the choice of these two constants. All other input data used to obtain the results in Fig. 14 were the same as for the previous simulations in this section.

For different combinations of $\omega_{\max}$ and r_h, the minimum value of $M_{\max}$ that can be used in Eq. (7) to obtain a successful arm deployment was chosen (Fig. 14). The two criteria for a successful arm deployment were as follows:

1) The arms were not allowed to retract more than 5% once fully deployed (i.e., $L_a > 0.95H$ for $t > t_1$, where t_1 was chosen as the first time when $L_a > 0.95H$).

2) The rotation of the center hub must not change direction during the deployment (i.e., $\omega_h > 0$ for all t).

The second criterion was shown to be the hardest. To take into account that FE simulations and real experiments give a more volatile behavior, the second criterion was augmented to $|\omega_h| > |\omega_{\max}/20|$ for all t.

The power required to apply this minimum torque is given by

$$P_j = M_j|\omega_j| \tag{36}$$

where $M_j = |M_h| = |M_f|$. The maximum power to the hub, $P_{h,\max}$, and to the flywheel, $P_{f,\max}$, required to apply the torque, defined by $M_{\max}$ and $\omega_{\max}$, is shown in Fig. 14. Because the flywheel rotated much faster, more power was required to apply the torque to the flywheel than to the hub. For the solid flywheel defined previously, the maximum power was about 10^4 times higher than for the previously defined hub–web–mass system. Thus, for these data, the

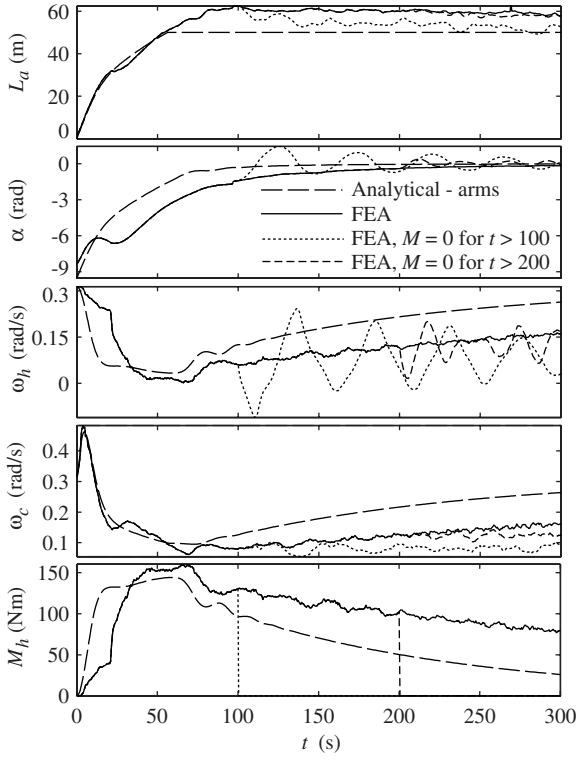

Fig. 13 Controlled one-step deployment of the space web.

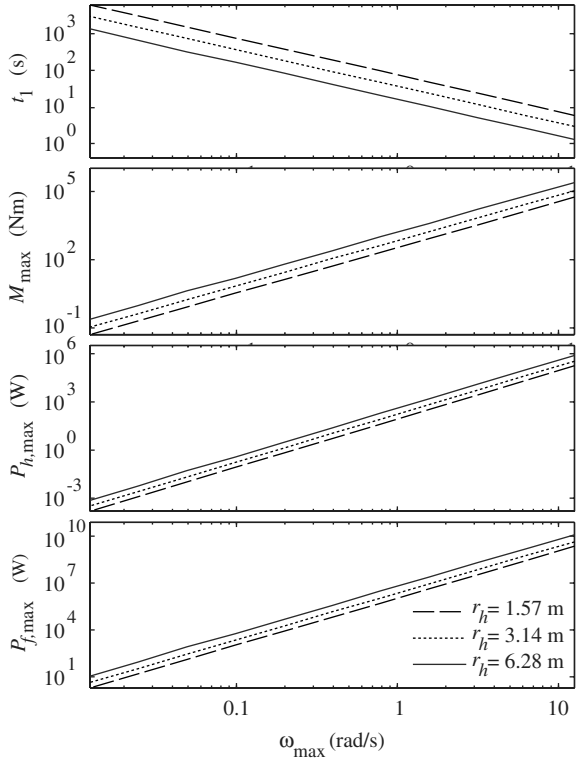

Fig. 14 Torque and power requirements for arm deployment times.

maximum power required by the electric motor was determined by the flywheel characteristics, and the same conclusion holds for arbitrary data for a solid flywheel with much smaller moment of inertia than the corresponding web.

The power capacity of the mission induces a constraint on the deployment velocity and deployment time. The deployment times ranged from less than 1 s for the largest r_h and $\omega_{\max}$ to hours for the smallest r_h and $\omega_{\max}$ in this example (Fig. 14). It is more interesting to study the dependence of the chosen parameters than the exact quantities, because the quantities vary also with other variables (e.g., the web size) and the hub, web, and corner masses. As expected, t_1 decreased linearly with increasing $\omega_{\max}$ or r_h, because the deployment velocity was increased linearly. $M_{\max}$ increased linearly with increasing r_h but quadratically with increasing $\omega_{\max}$, because the control law for M, where $M_{\max}$ is defined, is dependent on $\omega_{\max}$. $P_{h,\max}$ also increased linearly with increasing r_h but cubically with increasing $\omega_{\max}$, because the power to the hub is dependent on both M_h and ω_h, which are both dependent on $\omega_{\max}$. $P_{f,\max}$ is proportional to $P_{h,\max}$, because equal flywheels were used in this example.

The torque and power required for the deployment of the whole web should be higher than for the deployment of arms only, but Figs. 10 and 13 indicate that ω_h decreases to similar values for the same maximum torque $M_{\max}$. Therefore, for the chosen data, the values in Fig. 14 are also good approximations of the requirements for one-step deployment, and so the analytical model can be used to estimate the power requirements of the system with good accuracy.

Conclusions

The simulations indicated that it is possible to deploy a continuous space web by applying a torque to the center hub. To obtain this, a torque control law that implies that the torque increases when the angular velocity of the hub decreases, and vice versa, was used. From the analysis, we concluded that it is important to carefully choose the parameters in the control law; the maximum angular velocity must be large enough to deploy the web within the required time, yet small enough to allow acceptable values of the maximum torque, and the maximum torque must be large enough to achieve a successful deployment, yet low enough to meet present torque and power capabilities.

The use of a control torque on the center hub requires that the web is in tension; otherwise, only the hub rotation is affected and the web is uncontrolled. The easiest and safest way to tension the web during the whole deployment seems to be to deploy it in just one step. Even though the one-step deployment is not perfectly modeled with the analytical model, similar values of the control law parameters could be used to obtain a controlled one-step deployment. A controlled deployment in two distinctive steps may be obtained if tethers are used to control the deployment velocity of the second step, but this is both more complicated and slower than the one-step deployment.

The rapidly computed three-degree-of-freedom model was shown to be a valuable tool for determining important mission parameters, such as the torque and power requirements for given deployment times with different hub and web masses and sizes. The same model can be used for spin deployment of quadratic membranes from the same folding pattern, and similar models can be used for other folding patterns and web or membrane geometries. The finite element model was required to more accurately predict the behavior of the web when the different steps were initiated and at full deployment. Because it was shown that the proposed torque could be used to control more complicated cases than first intended, there is a possibility that it can also be used to control the spin deployment for other complicated folding cases for webs and membranes.

Experiments are required to verify the viability of the proposed folding and deployment. Entanglement is always a high risk factor for the deployment of this type of structure. Entanglements are difficult to model, but the risk is substantially decreased if the folding and release of the web from the center satellite can be performed properly.

Acknowledgments

Financial support from the ESA Advanced Concepts Team (ACT) during the first part of this work is gratefully acknowledged. In particular, we thank Dario Izzo, Claudio Bombardelli, and Leopold Summerer at ACT for ideas and discussion during that period.

References

[1] Jones, T. C., Bart-Smith, H., Mikulas, M., and Watson, J., "Finite Element Modeling and Analysis of Large Pretensioned Space Structures," *Journal of Spacecraft and Rockets*, Vol. 44, No. 1, 2007, pp. 183–193. doi:10.2514/1.23116

[2] Melnikov, V. M., and Pichkhadze, K. M., "Design of Frameless SA Deployed by Centrifugal Forces and Its Deployment Mechanism as a Basis Of New Technology of In-Orbit Power Plant Assembling," *Proceedings of the 56th International Astronautical Congress*, Vol. 6, IAC-05-C2.P.01, International Astronautical Federation, Paris, Oct. 2005, pp. 3972–3977.

[3] Schuerch, H. U. and MacNeal, R., "Deployable Centrifugally Stabilized Structures for Atmospheric Entry from Space," NASA CR-69, July 1964.

[4] Schuerch, H. U., and Hedgepeth, J. M., "Large Low-Frequency Orbiting Radio Telescope," NASA CR-1201, Oct. 1968.

[5] Kyser, A. C., "Uniform-Stress Spinning Filamentary Disk," *AIAA Journal*, Vol. 3, No. 7, 1965, pp. 1313–1316.doi: 10.2514/3.3129

[6] Robbins, W. M., Jr.,, "The Feasibility of an Orbiting 1500-Meter Radio Telescope," NASA CR-792, June 1967.

[7] MacNeal, R. H., "The Heliogyro: An Interplanetary Flying Machine," NASA CR-84460, March 1967.

[8] Hedgepeth, J. M., MacNeal, R. H., and Schuerch, H. U., "Heliogyro Solar Sailer Summary Report," NASA CR-1329, June 1969.

[9] Lang, W. E., and Honeycutt, G. H., "Simulation of Deployment Dynamics of Spinning Spacecraft," NASA TN-D-4074, Aug. 1967.

[10] Hedgepeth, J. M., "Dynamics of a Large Spin-Stiffened Deployable Paraboloidal Antenna," *Journal of Spacecraft and Rockets*, Vol. 7, No. 9, 1970, pp. 1043–1048. doi:10.2514/3.30100

[11] Melnikov, V. M., and Koshelev, V. A., *Large Space Structures Formed by Centrifugal Forces*, 1st ed., Vol. 4, Earth Space Institute Book Series, Gordon and Breach, Amsterdam, 1998, pp. 21–61.

[12] Shpakovsky, N., "Space mirror," *The TRIZ Journal* [online journal], Vol. 7, No. 6, 2002, http://www.triz-journal.com/archives/2002/06/e/index.htm [retrieved 20 Feb. 2008].

[13] Kishimoto, N., Natori, M. C., Higuchi, K., and Ukegawa, K., "New Deployable Membrane Structure Models Inspired by Morphological Changes in Nature," *47th AIAA/ASME/ASCE/AHS/ASC Structures, Structural Dynamics, and Materials Conference*, Vol. 5, AIAA, Reston, VA, 2006, pp. 3722–3725; also AIAA Paper 2006-1898.

[14] Wallace, R. A., Ayon, J. A., and Sprague, G. A., "Interstellar Probe Mission/System Concept," *IEEE Aerospace Conference Proceedings*, Vol. 7, Inst. of Electrical and Electronics Engineers, Piscataway, NJ, Mar. 2000, pp. 385–396.

[15] Salama, M., White, C., and Leland, R., "Ground Demonstration of a Spinning Solar Sail Deployment Concept," *Journal of Spacecraft and Rockets*, Vol. 40, No. 1, 2003, pp. 9–14. doi:10.2514/2.3933

[16] Burton, R. L., Coverstone, V. L., Hargens-Rysanek, J., Ertmer, K. M., Botter, T., Benavides, G., Woo, B., Carroll, D. L., Gierow, P. A., Farmer, G., and Cardin, J., "UltraSail—Ultra-Lightweight Solar Sail Concept," 41st AIAA/ASME/SAE/ASEE Joint Propulsion Conference, Tucson, AZ, AIAA Paper 2005-4117, July 2005.

[17] Mitsugi, J., Natori, M., and Miura, K., "Preliminary Evaluation of the Spinning Solar Sail," 28th AIAA/ASME/ASCE/AHS/ASC Structures, Structural Dynamics, and Materials Conference, AIAA Paper 1987-742, Monterey, CA, Apr. 1987.

[18] Matunaga, S., Mori, O., Nakaya, K., Iai, M., Omagari, K., and Yabe, H., "New Spinning Deployment Method of Large Thin Membranes with Tether Control," *54th International Astronautical Congress*, Vol. 1, IAC-03-A.4.01, International Astronautical Federation, Paris, Sept.–Oct. 2003, pp. 257–260.

[19] Matunaga, S., Yabe, H., Nakaya, K., Iai, M., Omagari, K., and Mori, O., "Membrane Deployment for Spinning Formation Flight Solar Sail," 14th ISAS/JAXA Workshop on Astrodynamics and Flight Mechanics, Tokyo, Japan Aerospace Exploration Agency Paper A-11, July 2004.

[20] Mori, O., Tsuda, Y., Nishimura, Y., and Kawaguchi, J., "Deployment Dynamics of Clover Type Solar Sail," 14th ISAS/JAXA Workshop on Astrodynamics and Flight Mechanics, Tokyo, Japan Aerospace

Exploration Agency Paper A-5, July 2004.
[21] Nakano, T., Mori, O., and Kawaguchi, J., "Stability of Spinning Solar Sail-Craft Containing a Huge Membranes," *AIAA Guidance, Navigation, and Control Conference*, Vol. 5, AIAA, Reston, VA, 2005, pp. 3425–3437; also AIAA Paper 2005-6182.
[22] Masumoto, S., Omagari, K., Yamanaka, T., and Matunaga, S., "System Configuration of Tethered Spinning Solar Sail for Orbital Experiment: Numerical Simulation and Ground Experiment," 25th International Symposium on Space Technology and Science (ISTS), Kanazawa City, Japan, Japan Aerospace Exploration Agency Paper 2006-d-21, June 2006.
[23] Tsuda, Y., Nakaya, K., Mori, O., and Yamamoto, T., "Microsatellite-Class Solar Sail Demonstrator—Mission Design and Development Status," 25th International Symposium on Space Technology and Science (ISTS), Kanazawa City, Japan, Japan Aerospace Exploration Agency Paper 2006-k-37, June 2006.
[24] Nakasuka, S., Aoki, T., Ikeda, I., Tsuda, Y., and Kawakatsu, Y., "'Furoshiki Satellite'—A Large Membrane Structure as a Novel Space System," *Acta Astronautica*, Vol. 48, Nos. 5–12, 2001, pp. 461–468. doi:10.1016/S0094-5765(01)00056-X
[25] Nakasuka, S., Funase, R., Nakada, K., Kaya, N., and Mankins, J. C., "Large Membrane 'Furoshiki Satellite' Applied to Phased Array Antenna and Its Sounding Rocket Experiment," *Acta Astronautica*, Vol. 58, No. 8, 2006, pp. 395–400. doi:10.1016/j.actaastro.2005.12.010
[26] Nakasuka, S., Funane, T., Nakamura, Y., Nojira, Y., Sahara, H., Sasaki, F., and Kaya, N., "Sounding Rocket Flight Experiment for Demonstrating 'Furoshiki Satellite' for Large Phased Array Antenna," *Acta Astronautica*, Vol. 59, Nos. 1–5, 2006, pp. 200–205. doi:10.1016/j.actaastro.2006.02.014
[27] Kaya, N., Iwashita, M., Nakasuka, S., Summerer, L., and Mankins, J., "Crawling ROBOTS ON Large Web in Rocket Experiment on Furoshiki Deployment," *Proceedings of the 55th International Astronautical Congress*, Vol. 10, IAC-04-R3, International Astronautical Federation, Paris, Oct. 2004, pp. 663–667.
[28] Nakasuka, S., and Kaya, N., "Quick Release on Experiment Results of Mesh Deployment and Phased Array Antenna by S-310-36," *The Forefront of Space Science* [online journal], 13 Apr. 2006, http://www.isas.ac.jp/e/forefront/2006/nakasuka/ [retrieved 4 Sept. 2006].
[29] Tibert, G., and Gärdsback, M., "Space Webs: Final Report," ESA Advanced Concepts Team, Rept. 05/4109a, Noordwijk, The Netherlands, 2006.
[30] McKenzie, D., Cartmell, M., Radice, G., and Vasile, M., "Space Webs: Final Report," ESA Advanced Concepts Team, Rept. 05/4109b, Noordwijk, The Netherlands, 2006.
[31] Palmerini, G. B., Sgubini, S., and Sabatini, M., "Space Webs Based on Rotating Tethered Formations," *Proceedings of the 57th International Astronautical Congress*, Vol. 10, IAC-06-D1.1.04, International Astronautical Federation, Paris, Oct. 2006, pp. 6819–6828.
[32] Gärdsback, M., Tibert, G., and Izzo, D., "Design Considerations and Deployment Simulations of Spinning Space Webs," *48th AIAA/ASME/ASCE/AHS/ASC Structures, Structural Dynamics, and Materials Conference*, Vol. 2, AIAA, Reston, VA, 2007, pp. 1503–1512; also AIAA Paper 2007-1829.
[33] McKenzie, D., and Cartmell, M., "Modelling of Tethered Space-Web Structures," *Journal of the British Interplanetary Society*, Vol. 61, Jan. 2008, pp. 24–31.
[34] Miyazaki, Y., and Iwai, Y., "Dynamics Model of Solar Sail Membrane," 14th ISAS/JAXA Workshop on Astrodynamics and Flight Mechanics, Tokyo, Japan Aerospace Exploration Agency Paper A-6, July 2004.
[35] Blomquist, R., "Solar Blade Nanosatellite Development: Heliogyro Deployment, Dynamics and Control," 13th Annual AIAA/USU Conference on Small Satellites, Logan, UT, Utah State Univ. Paper VII-3, Aug. 1999.
[36] Bergamin, L., and Izzo, D., "Comments on Deployment and Control of Charged Space Webs," ESA Advanced Concepts Team, Rept. ACT-TNT-MAD-CDCCSW07, Noordwijk, The Netherlands, Sept. 2007.
[37] Genta, G., *Kinetic Energy Storage*, 1st ed., Butterworths, London, 1985, p. 69.
[38] Babuska, V., Beatty, S. M., deBlonk, B. J., and Fausz, J. L., "A Review of Technology Developments in Flywheel Attitude Control and Energy Transmission Systems," *2004 IEEE Aerospace Conference Proceedings*, Vol. 4, Inst. of Electrical and Electronics Engineers, Piscataway, NJ, Mar. 2004, pp. 2784–2800.
[39] Miura, K., "Method of Packaging and Deployment of Large Membranes in Space," 31st International Astronautical Congress, International Astronautical Federation Paper IAF-80-A31, Sept. 1980.
[40] Horner, G., and Elliott, M., "A Fabrication and Deployment Approach for a Miura-Ori Solar Sail Model," 43rd AIAA/ASME/ASCE/AHS/ASC Structures, Structural Dynamics, and Materials Conference, AIAA Paper 2002-1708, Denver, CO, Apr. 2002.
[41] Furuya, H., Inoue, Y., and Masuoka, T., "Concept and Deployment Characteristics of Rotationally Skew Fold Membrane for Spinning Solar Sail," 14th ISAS/JAXA Workshop on Astrodynamics and Flight Mechanics, Tokyo, Japan Aerospace Exploration Agency Paper A-3, July 2004.
[42] Guest, S. D., and Pellegrino, S., "Inextensional Wrapping of Flat Membranes," *Proceedings of the 1st International Seminar on Structural Morphology*, International Association for Shell and Spatial Structures, Madrid, Sept. 1992, pp. 203–215.
[43] Scheel, H. W., "Space-Saving Storage of Flexible Sheets," U.S. Patent 3,848,821, 19 Nov. 1974.
[44] Watanabe, H., Natori, M. C., Okuizumi, N., and Higuchi, K., "Folding of a Circular Membrane Considering the Thickness," 14th ISAS/JAXA Workshop on Astrodynamics and Flight Mechanics, Tokyo, Japan Aerospace Exploration Agency Paper A-4, July 2004.
[45] Banik, J., and Murphey, T., "Synchronous Deployed Solar Sail Subsystem Design Concept," 48th AIAA/ASME/ASCE/AHS/ASC Structures, Structural Dynamics, and Materials Conference, Vol. 2, Honolulu, HI, AIAA Paper 2007-1837, Apr. 2007, pp. 1590–1602.
[46] MATLAB, Software Package, Ver. R2007b, The Mathworks, Inc., Natick, MA, 2007.
[47] LS-DYNA, Software Package, Ver. 471/7600.1224, Livermore Software Technology Corp., Livermore, CA, 2007.
[48] Hallquist, J. O., *LS-DYNA Theory Manual*, Livermore Software Technology Corp., Livermore, CA, 2006.
[49] Hughes, T., Taylor, R., Sackman, J., Curnier, A., and Kanoknukulchai, W., "A Finite Element Method for a Class of Contact-Impact Problems," *Computer Methods in Applied Mechanics and Engineering*, Vol. 8, No. 3, 1976, pp. 249–276. doi:10.1016/0045-7825(76)90018-9doi:
[50] Adoum, M., and Lapoujade, V., "Examples Manual for *USER LOADING Option," 4th European LS-DYNA Users Conference, Ulm, Germany, DYNAmore Paper G-I-29, May 2003.
[51] Seely, L. G., Zimmerman, M., and McLaughlin, J., "The Use of Zylon Fibers in ULDB Tendons," *Advances in Space Research*, Vol. 33, No. 10, 2004, pp. 1736–1740. doi:10.1016/j.asr.2003.07.046